Porous Ni@Tantalum Silicate as a Tandem Catalyst for Selective Synthesis of C_4 Hydrocarbons from Ethanol

M.G. Sibi, Hari Singh and Anil K. Sinha*

CSIR-Indian Institute of Petroleum, Dehradun - 248005, India

Abstract: Selective catalysts for sustainable production of fuels and commodity chemicals are important due to the abundance of the raw materials in the nature. Most of these reactions require multiple active sites due to the complexity of the reactions involved. In view of this, we have synthesized a multifunctional catalyst for the selective synthesis of C_4 hydrocarbons from ethanol. The reason for selecting ethanol is due to the easy production and transformation of biomass, and the heavy demand in future for fuels. Here, we have synthesized nanometer sized nickel particles and protected it with a porous siliceous cover. The acidity of the catalyst has been tuned by introducing tantalum in the framework structure. The use of easily available metals for the synthesis of catalysts reduces the cost of making the catalyst and it also gives high temperature resistance characteristics. The physico-chemical characteristics of the catalysts were studied with various sophisticated instruments. We also investigated in detail the selective production of C_4 hydrocarbons, by tuning the reaction conditions.

Keywords: Catalyst, ethanol, hydrocarbons, silicate, sugar, synthesis.

INTRODUCTION

Depletion of the hydrocarbon base stocks may cause huge problems not only in the fuel field, but also in fine chemicals, polymers, solvents *etc.* [1, 2]. Replacement of fossil fuels with alternative sources of energy is clearly necessary, but presents the world with an unprecedented technical challenge. Alternative fuels produced from traditional fuel sources may be an important intermediate step in the transition to new fuel and chemical sources [3]. In the wide scope of this, researchers are looking for the production of these materials from renewable feed stocks. Lignocellulosic biomass has three different components, lignin, hemicellulose and cellulose, and all these can be converted into useful chemicals. Due to the food versus fuel issue, the production of these chemicals from edible-renewables is to be strictly abandoned and due to this, researchers mainly focus on three different routes i.e. lignocellulosic sugar to fuels and chemicals [3-7], pyrolysis of biomass [8-10], and the lipid based production [11]. Most of these products can also be upgraded for further value-addition. But new technologies and processes are needed to achieve these goals [12].

The on and off road demands for biofuels are to reach 107 million tons in 2025 [13]. At the same time, the application of ethanol as biofuel at present is 7 billion liters, which is to reach 133 billion liters. [14] Currently, it is blended with gasoline and used as transportation fuel. It can be easily transformed into various chemicals like 1,3-butadiene, crotanaldehyde, n-butanol, diethyl ether, *etc.* [15-21]. Not only this, industrially necessary ethylene and propylene can also be easily produced from ethanol, and these are very important raw materials for petrochemical and polymer industry [22-24]. Nowadays, these are produced from the steam cracking of naphtha. Goto *et al.* selectively produced propylene from ethanol on alkaline earth metal supported H-ZSM-5 zeolites [25]. Maderia *et al.* used various zeolites for the conversion of ethanol to commodity chemicals [26]. They have reported various ranges of products with almost 100 % conversion but with poor selectivity. Tsuchida *et al.* synthesized 2-butanol from ethanol with 50 % conversion on hydroxyapatite [27]. But, C_4 hydrocarbons, mainly butanes and butenes, are also very important as fuel and raw materials for various chemicals. Recently, Sen *et al.* used butenes as one of the raw material for the production of biofuels [28]. They treated the levulinic acid, obtained from the biomass conversion process, with butenes to produce Sec-butyl levulinate and sec-butyl formate. The unreacted butene hydrolysed to form 2-butanol. Finally, they produced, with various catalysts, the oligomers of butenes having C_8 to C_{20} alkene species. So, various catalyst systems are required for the selective synthesis of hydrocarbons from ethanol.

Porous materials having tunable properties are important not only for conversion but also for selectivity. Basic sites in the catalyst can selectively produce butadienes, butanol etc. and at the same time highly acidic catalysts can produce ethylene, propylene, aromatics etc. So, the material can be selected according to the requirement of chemical to be produced. On the basis of this, metals on porous metal oxides have great importance due to their high reactivity. In addition, the incorporation of the second metal in the framework gives acidic nature to the material, which can be controlled by varying the metal ratios. Recent literature reveals that the active metals in the nanometer range with particular shapes enhance the activity of the catalyst [29, 30]. But, at the same time they have large tendency to

*Address correspondence to this author at the CSIR-Indian Institute of Petroleum, Dehradun - 248005, India; Tel:+91-1352525842; Fax:+91-135-266-203; E-mail: asinha@iip.res.in

1876-214X/14

agglomerate at high reaction temperature, so their activity is lost very quickly. This can be overcome by protecting it with an outer cover (core-shell structure) and it prevents the agglomeration, meanwhile the shell also requires pores for the easy diffusion of the reactants and products.

Here, we are reporting the synthesis of a novel mesoporous tantalum silicate catalyst for the selective production of C_4 hydrocarbons from ethanol. We are trying to tailor multifunctional properties like, acidity, dehydration ability, easy diffusion of the reactants and products, and provide high temperature stability to the catalyst. The highly active nickel nanoparticles have been synthesized and protected with layers of silica. The acidic nature of the catalyst was developed by the incorporation of a second metal tantalum inside the framework. To the best of our knowledge, this is the first reported highly selective catalyst for the selective transformation of the ethanol to butane and butenes. We have also studied in detail, the effect of temperature and reaction time on the catalyst selectivity.

MATERIALS AND METHODS

Nickel nitrate hexahydrate, hydrazine hydrate, ethanol and ammonia were purchased from Merck India. Tantalum chloride, cerium nitrate, tetra-ethyl orthosilicate (TEOS) and Triton-x were purchased from Aldrich Chemicals. Deionized water used was obtained from Hi-Media laboratories. The synthesis of the catalyst was carried out by a simple solvothermal method. In a typical synthesis a 1:1 solution of water and toluene (50 ml each) was thoroughly stirred with 2 g of Triton-X for 3 hours at 70°C followed by the addition of 1 mmole of nickel nitrate in 10 ml water dropwise and continuous stirring for 30 minutes. The entire solution was reduced by adding 6 ml hydrazine hydrate, and heated for 1 hour (a purple colored solution was obtained). Both the solutions of tantalam chloride (300 mg in 10 ml ethanol) and TEOS were added drop wise to the above solution simultaneously. The above solution is continually stirred and heated for additional 3 hours, after adding 20 ml 33 % ammonia solution. After the completion of reaction the precipitates were filtered and washed with water and dried overnight and calcined at 600°C for 8 hours at 1°C/min. For comparison, Ni@Cerium silicate was prepared by similar method using cerium nitrate.

Characterization of the Catalyst

The physico-chemical properties of the catalyst were determined by X-ray diffraction (XRD), scanning electron microscopy (SEM), and temperature programmed reduction (TPR) etc. X- ray diffraction patterns were obtained using Cu Kα radiation (40 kV and 40 mA, Advanced Bruker D8 diffractometer). The textural properties of catalysts were determined by N_2 adsorption-desorption isotherms at 77 K (BelsorbMax, BEL, Japan) and the related data (surface area, S_{BET}; pore volume, V_T; pore diameter) were calculated by standard methods. The FT-IR analysis was performed on Perkin Elmer 1760 X spectrometer with KBr pellets. The SEM images were realized on field emission scanning electron microscope, FEI Quanta 200 F, using tungsten filament doped with lanthanum hexaboride (LaB_6) as an X-ray source, fitted with an ETD detector under high vacuum mode using secondary electrons and an acceleration voltage of 10 or 30 kV. Catalysts were analyzed by spreading them on a carbon tape. Energy-dispersive X-ray spectroscopy (EDAX) was used in combination with SEM for elemental analysis. The elemental mapping was conducted with the same spectrometer. The TEM images were taken on a Hitachi H7100 electron microscope operated at 75 KV. The samples were suspended in ethanol and sonicated for 5 minutes and placed on a copper grid for analysis. The amount and strength of the acid sites were measured by ammonia adsorption-desorption technique using a chemical adsorption instrument, Micrometrics 2900 with a thermal conductivity detector. About 0.20 g sample was saturated with NH_3 at 120 °C, then flushed with helium to remove the physically adsorbed NH_3. Finally, the desorption of NH_3 was carried out at a heating rate of 10 °C/min under helium flow. Thermal stability of the material was studied by TG and DTA analysis under nitrogen atmosphere with a ramping temperature of 10°C/min using Perkin Elmer equipment. Surface oxidation state of the catalyst was analyzed by X-ray photoelectron spectroscopy.

Evaluation of the Catalyst Activity

The activity of the catalyst was studied in continuous flow, fixed bed reactor from HiTech, India. The catalyst (1 gm) was loaded into a tubular reactor having an internal diameter of 0.8 cm with a length of 46 cm. To keep the catalyst in the middle, the top and bottom of the reactor was filled with SiC. Finally, powdered catalyst (by grinding) was used to minimize the mass transfer limitations. The catalyst was mixed with SiC to overcome the heat transfer limitations on the bed. Using finally powdered catalyst, constant temperature throughout the catalyst bed was maintained. A wide range of space velocities and temperatures were used to find the conditions for maximum conversion and yield. The experiments were carried out with a single zone tubular furnace at space velocities (LHSV) of 1-5 h^{-1} and reaction temperatures of 100-400°C. The reaction products were passed through a condenser, before the high pressure separator. The products were analyzed by an online Gas chromatograph (Agilent) connected to the reactor. For avoiding errors, the reaction temperature was increased at the rate of 1°C/min, and kept at the desired temperature for 1 hour, and then the products were analyzed.

RESULT AND DISCUSSION

Typical powder X-ray diffraction patterns of the catalyst are shown in Fig. (**1**). It can be observed from the figure that the material is amorphous in nature. The wide peak present at 23° and seen as a broad band between 20-30° is due to amorphous silica. Low angle XRD analysis did not show any peaks due to mesoporous structure. The porous properties of the catalysts were studied by N_2 adsorption-desorption isotherms, at 77 K. The adsorption-desorption isotherms and the pore size distribution curves are shown in Fig. (**2**). The other physico-chemical properties of the catalysts are listed in Table **1**. From the results it can be observed that the material shows type III isotherm having H1 hysteresis loop with multiple pores. This type of hysteresis loop indicates that the material has internal porous structure [31]. The late

and steep adsorption steps show the relatively large pore size distribution. The pore size distributions were calculated from the adsorption isotherm, using BJH method, and are shown in Fig. (**2**). It can also be observed from the figure that the material has broad pore size distribution in the range 20-150 nm.

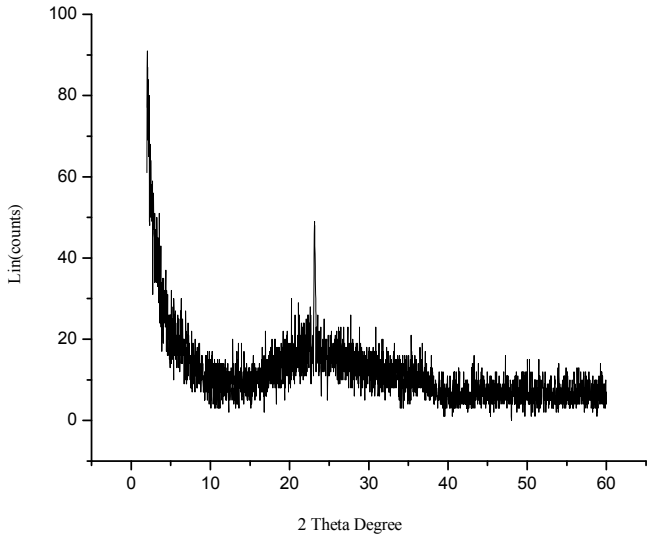

Fig. (1). Wide angled XRD pattern of the catalyst.

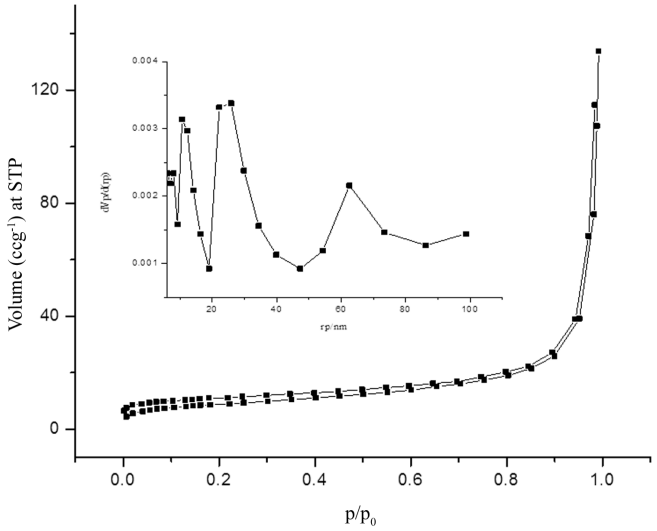

Fig. (2). N_2 Adsorption desorption isotherm & BJH pore size distribution of the catalyst.

FTIR analysis was carried out to evaluate the structure and bonding of the material and is shown in Fig. (**3**). Bonding of the metals inside the framework is important for tailoring the properties to direct the activity of the catalyst. In view of this the most important peak present in the spectrum is at about the wave numbers 2335 cm^{-1} and 1025 cm^{-1}. The peak at 2335 cm^{-1} may correspond to the Ta=O bond and 1025 cm^{-1} to the bending vibration of Si-O-Ni [32]. The positions of the peak present at 1097.5 cm^{-1} is generally due to the tetrahedral silica framework of the material [33]. In pure silica the original Si-O-Si vibration is at 1106 cm^{-1}, but due to the presence of tantalum in Si-O-Ta linkages in the framework, it may have shifted to 1097 cm^{-1}. Another important peak present in the spectrum is at 470 cm^{-1} which is due to the presence of Ta-O-Ta linkages in the framework. The other peaks at 804 cm^{-1} and 3434 cm^{-1} may correspond to the stretching vibration of the Si-O-Si bond and of the OH of the adsorbed water, respectively.

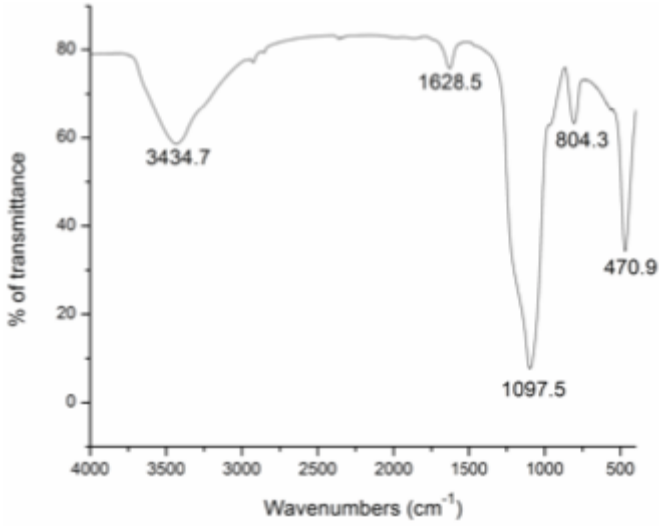

Fig. (3). FTIR Spectrum of the Catalyst

The morphologies of the synthesized catalysts were examined by scanning electron microscope (SEM). The representative SEM image of the catalyst is shown in Fig. (**4a**). It can be observed from the figure that the synthesized material has spherical particles with slight agglomeration. The EDAX analysis shows (Fig. **5**) that the material has approximately 29.9 % silica, 2.5 % nickel and 2.9 % tantalum (atomic %). The elemental mapping of the catalyst reveals a homogeneous distribution of all the components (Fig. **6**). From these figures, it can be seen that nickel appears to be in lower amount than tantalum even though they are in similar amounts which indicates that the nickel is covered by silica and tantalum is on the surface. The in-depth morphology of the material was studied by TEM analysis and is shown in Fig. (**4b**). The shape of nickel nanoparticles can be clearly visualized from this figure. It can also be visualized from the TEM image that the Ni particles are covered with tantalum-silica coating (Fig. **4c**). It prevents the nickel particles from agglomeration.

Adsorption of NH_3 was used to determine the acidity of the catalysts. It provides the total acidity (Table **1**) of the acid sites. Fig. (**7**) shows the NH_3 -TPD curves of the catalysts calcined at 600°C. Both strong and weak acid sites present in the catalyst can be visualized from the graph. A strong peak present in between 180 to 300°C may be attributed to the presence of weak and medium acid sites,

Table 1. Surface properties of the catalyst.

Catalyst	Surface Area	Pore Volume	Surface Acidity	Pore Size
Ni@Tantalam silicate	69 m^2g^{-1}	0.193 ml g^{-1}	0.188 mmol/gram	10-150 nm

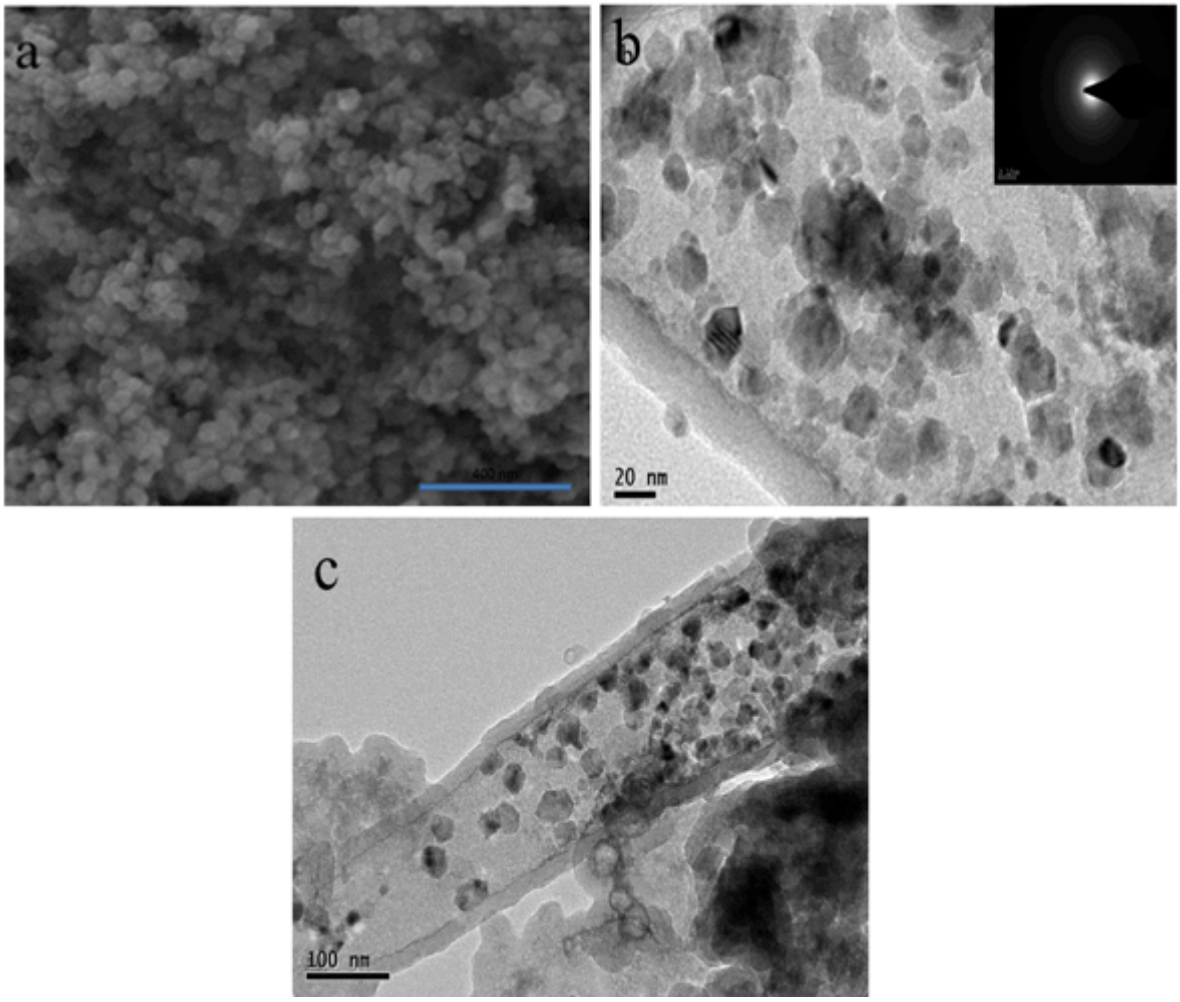

Fig. (4). SEM (**a**) & TEM (**b**) images of the catalyst.

and the peak between 600 to 900°C might be due to the presence of strong acid sites. We also observed that the total acidity of the catalyst is comparatively low, but the peaks due to strong and weak acid sites are well separated. The acidic SiO_2-TaO_2 support is expected to act as ethanol dehydration site in the catalyst [34, 35].

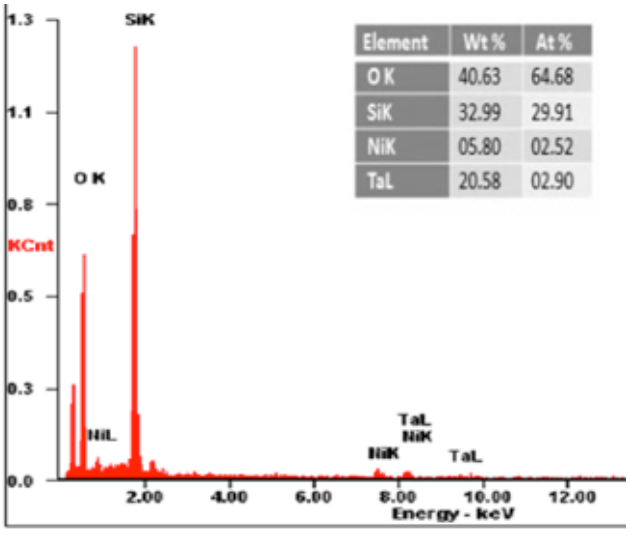

Element	Wt %	At %
O K	40.63	64.68
SiK	32.99	29.91
NiK	05.80	02.52
TaL	20.58	02.90

Fig. (5). EDAX of the Catalyst

Thermal stability of the material was studied by TGA/DTA analysis under nitrogen atmosphere. The results obtained are shown in S1 (supporting figure). It can be observed from the figure that the total weight loss of the material from 25 to 900°C was below 20 %. From the close analysis of the TG graph it may be concluded that the weight loss (10 %) from 0 to 200°C, may be due to the loss of adsorbed water in the material. A sharp weight loss of approximately 3% can be observed at 220°C, which may be due to the removal of oxygen from the framework with a phase change of the material, which is confirmed from the DTA curve. A very gradual weight loss was also observed up to the temperature of 900°C. From these overall results, it may be concluded that the material possesses high thermal stability.

Different surface chemical states of the catalyst have been analyzed by X-ray photoelectron spectroscopy as shown in Fig. (**8**). Oxidation states of the metals presents in the materials can be determined from the binding energies and their corresponding chemical shifts. Fig. (**8a**) is the representative XPS spectra of nickel (Ni $2p_{3/2}$) of the catalyst. It can be seen from the figure that nickel is present in various oxidation states. The peak at 852.6 corresponds to the zero oxidation state, whereas Ni^{2+} is observed at 854.6 eV

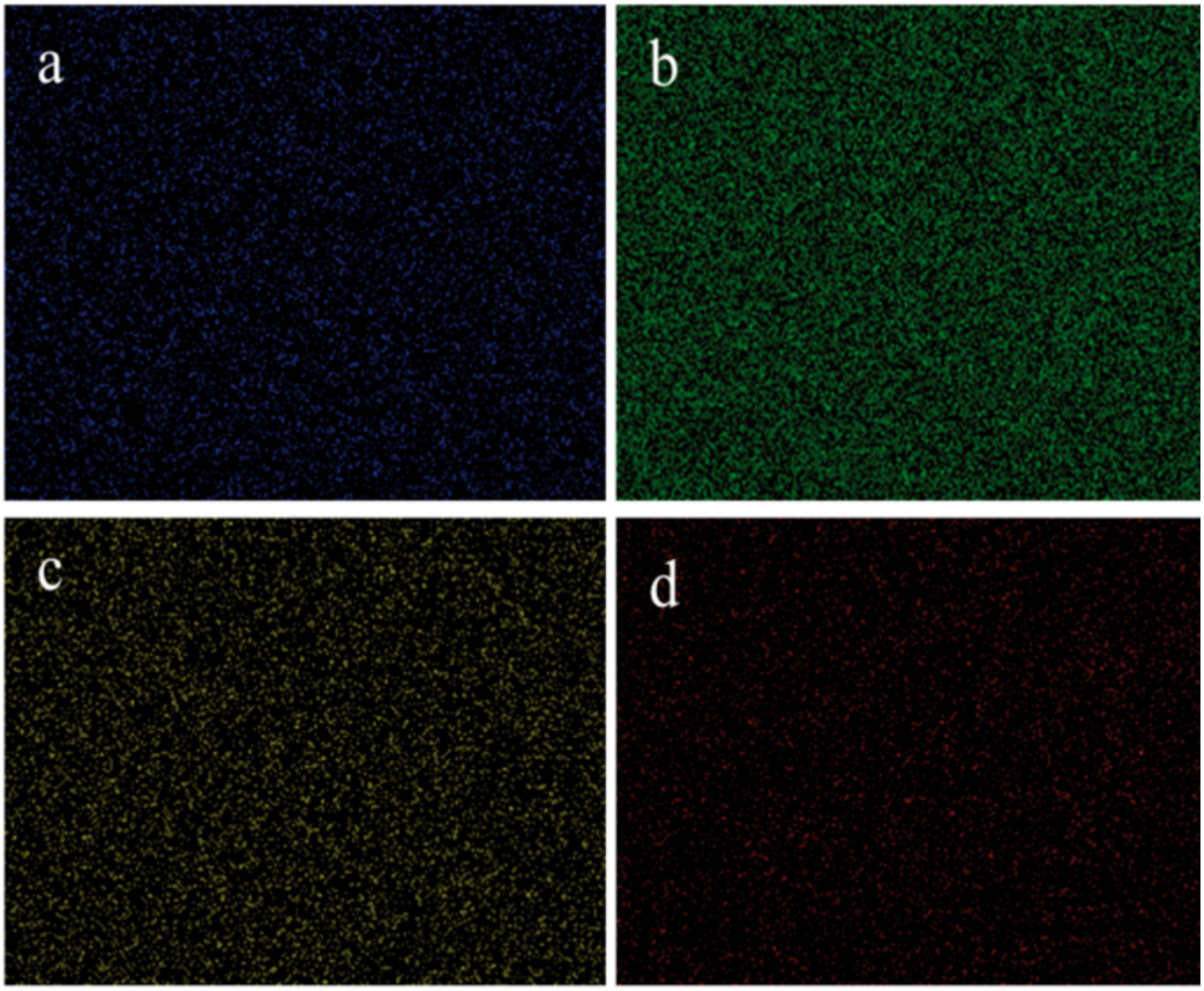

Fig. (6). Elemental mapping of the catalyst: (**a**) Nickel, (**b**) Silica, (**c**) Tantalum, (**d**) Oxygen.

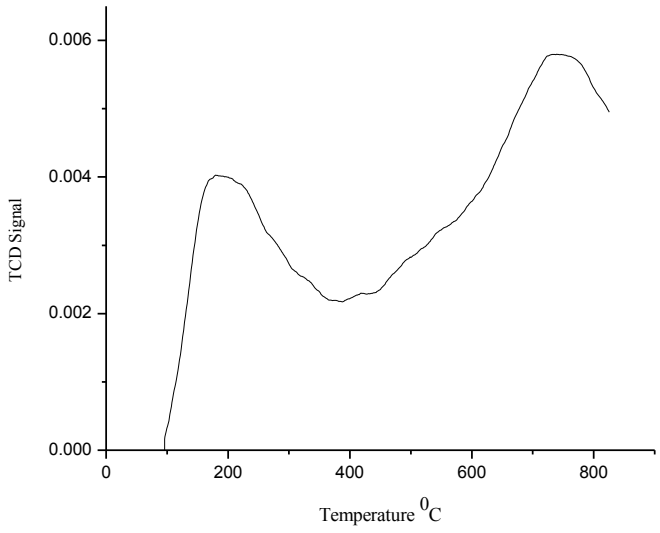

Fig. (7). TPD of the catalyst.

and Ni^{3+} at 856.1 eV. XPS spectra of the Ta $4f_{5/2}$ and Si $2s_{1/2}$ are shown in Fig. (**8b**). Considering the binding energy results, the oxidation states may be concluded to be +4 and +3 for tantalum and +4 for Si. From these results, it can be concluded that silicon and tantalum are present as SiO_2 and TaO_2, whereas nickel is present both in metallic and oxidized states. Nickel in metallic, Ni° state could be the hydrogenation center, while the oxidic nickel (NiO), may catalyze carbon-carbon bond formation reactions.

We have studied the ethanol conversion reaction from low temperature to high temperature at various space velocities. A wide range of space velocities and temperatures were used to find the conditions for maximum conversion and yield. The reaction was carried out in vapor phase and the mass transfer limitations were minimized by the extra large pores (10-150 nm size) present in the catalyst. Wide range of space velocities and temperatures were studied to optimize the conditions for maximum conversion and yields. Since the transfer hydrogenation is an important intermediate reaction step, we utilize the hydrogenation activity of the nickel. XPS analysis as discussed above confirmed the presence of metallic nickel in the catalyst. For protecting the hydrogenation activity we encapsulated the nickel inside a

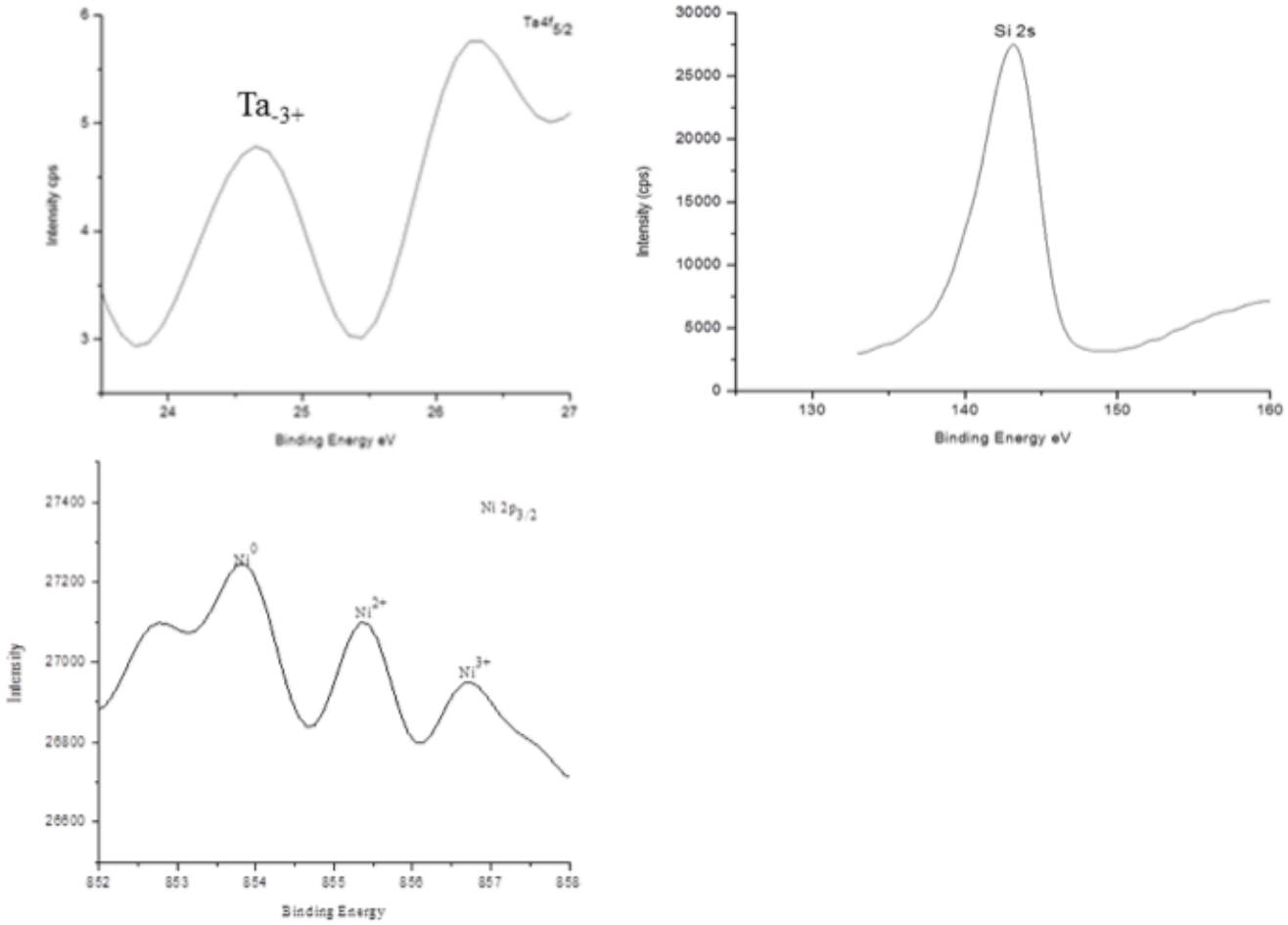

Fig. (8). XPS spectra of the catalyst.

porous material and it has been made by mixed oxides of tantalum with silica. Acidity of the catalyst is the driving force in many of the selective reactions of ethanol transformation. Due to the presence of strong acidity in the catalyst as observed by ammonia TPD study (due to TaO_2-SiO_2 type mixed supports), ethanol has converted mainly to ethylene by dehydration reaction. A lot of side products like aromatics, alkanes, diols etc. were also produced. But selectivities for these products were very low. Our novel catalyst has mild and strong acidity, with an overall acidity of 0.188 mmol/g. It favors the selective production of C_4 hydrocarbons. The porous nature of the catalyst favors easy diffusion of the reactants and products. Due to the presence of the highly active sites for the dehydration and combination of the intermediates, we have achieved approximately 98 % conversion in almost all the ranges of the reaction temperatures, at various space velocities. Other information obtained from the analysis was the selectivity towards the carbon monoxide and carbon dioxide. Both the gases were observed at low temperature as well as high temperature. When the reaction is performed at moderate temperature, the removal of oxygen takes place through the formation of water molecules and no CO and CO_2 is found. It means that by controlling the reaction temperature, we can avoid the formation of the CO and CO_2.

For elucidating activity and selectivity of the catalyst, we have conducted an experiment at a space velocity of $1h^{-1}$ and at temperatures from 100°C to 400°C. The results obtained are represented in Fig. (**9**). It was observed that several products were obtained, with some surprising results. When the temperature was 100°C, C_4 and C_3 with 1-butene and propylene were predominant. On increasing the temperature from 150°C to 275°C, the catalyst selectively produces isobutane and n-butane. When the temperature reached to 350°C, the trend is shifted to maximum C_4 hydrocarbons i.e. the production of iso-butane was maximum. On the other hand, the production of ethylene started at 300°C and continuously increased up to 400°C. The low percentage of methane and ethane confirmed the transfer hydrogenation on the catalyst.

To study the effect of space velocity on the reactivity of the catalyst, we doubled the space velocity to $2h^{-1}$. The result obtained were compiled and represented in Fig. (**10**). When the temperature increased, the presence of n-butane also increased and was maximum at 250°C. Again, it can be seen from the results that on increasing the temperature to 400°C, the selectivity of C_4 hydrocarbons decreased, with an increase of other by-products. One of the notable results was the formation of the C_5 hydrocarbons on the catalyst. The maximum production of i-pentane was observed at 300°C, and at all other temperatures the C_5 hydrocarbon production was nearly constant. The presence of ethylene also showed the same trend as at the space velocity of $1h^{-1}$.

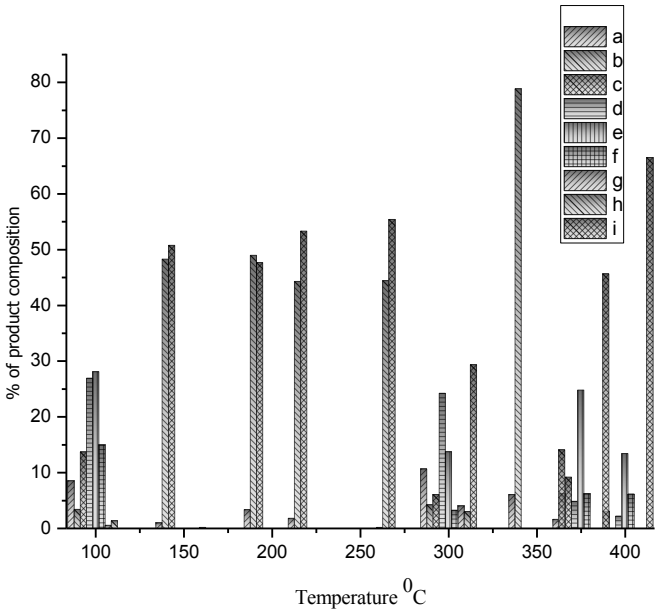

Fig. (9). Percentage of Hydrocarbons Vs Temperature at LHSV $1h^{-1}$ (a: ethylene, b, iso-butane, c: n-butane,d:1-butene, e: 2-butene, f: t-2 butene, cis 2-butene, h: iso-pentane, i: n-pentane).

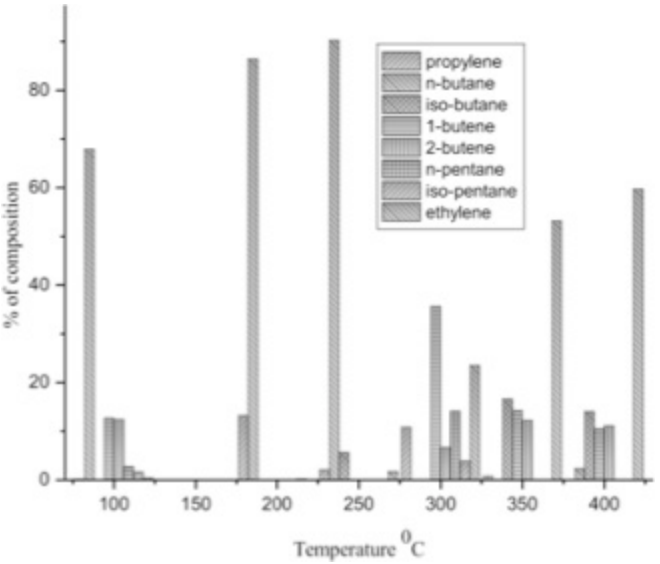

Fig. (10). Percentage of hydrocarbons at different reaction temperatures at $2h^{-1}$ LHSV.

On the basis of the above results, we conducted reaction at slightly higher space velocities ($4h^{-1}$ and $5h^{-1}$) and at slightly higher temperature. The results obtained are represented in Figs (**11**, **12**). Due to the incomplete conversion, we have omitted the results up to 300°C. From the figure it is observed that the selectivity of C_4 hydrocarbons was continuously increasing. The other important result obtained in this figure is the formation of n-butane. The percentage production of this important hydrocarbon increased with the increase of temperature. But when the side product cis-2-butene was formed, the

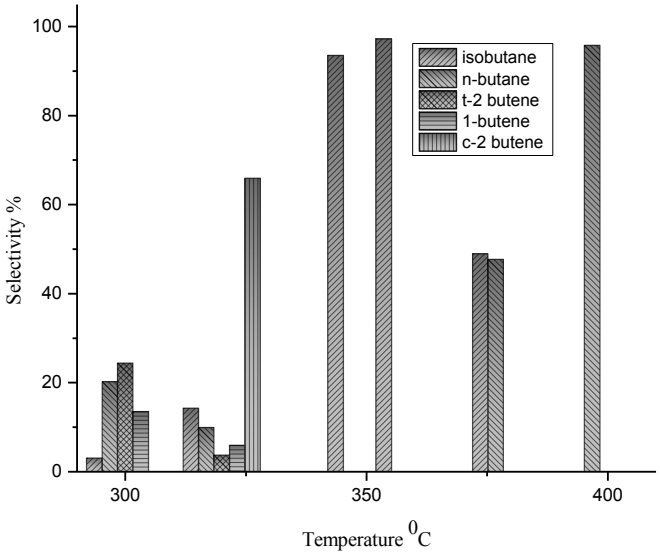

Fig. (11). Percentage of hydrocarbons at different reaction temperatures at $4h^{-1}$ LHSV.

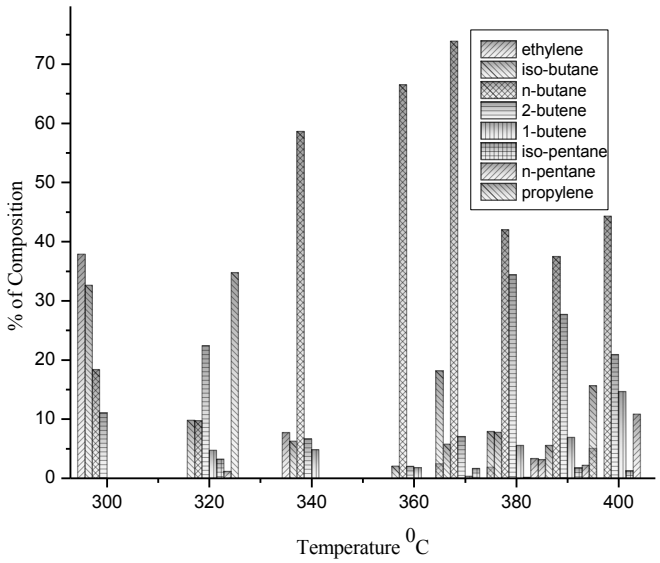

Fig. (12). Percentage of hydrocarbons at different reaction temperatures at $5h^{-1}$ LHSV.

production of n-butane was almost diminished and the production of propylene was predominant. When trans-2 butene was present in the product stream, n-butane was predominant. In the detailed analysis of the results, we found that the maximum selective production of n-butane was observed at 370°C and after that a slight decrease in the selectivity was noted. The presence of n-pentane and i-pentane was also observed with same trend in the product stream as in our previous experiments. From these results it can be concluded that by careful optimization of the reaction conditions, it is possible to make different products selectively. Tantalum free silica sample will not have the required acidity for dehydration of ethanol which results in direct cracking and rapid coking without formation of desired hydrocarbons. To study the effect of metal on the framework instead of tantalum ceria is incorporated and the

results obtained were represented in Fig. (**13**). It can be observed from the figure that upon changing, the metal the selectivity turns to C_2 hydrocarbons and insignificant yield of desired higher hydrocarbons is observed. Lower acidity for Ni@Cerium silicate than that for the Ni@Tantalum silicate is probably responsible for the difference.

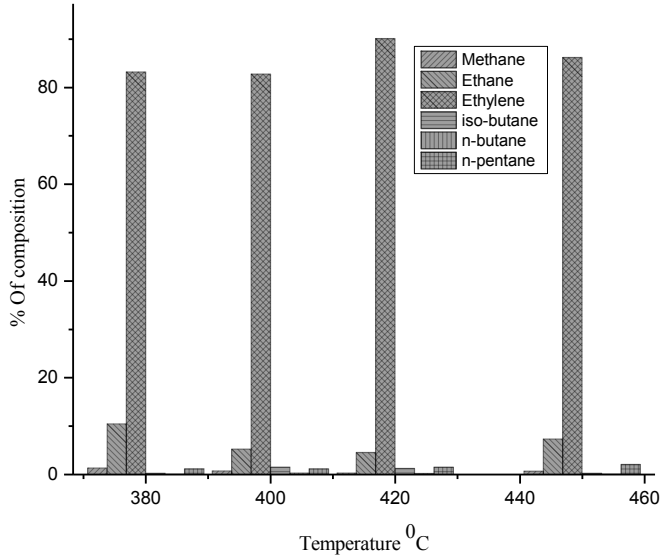

Fig. (13). Percentage of hydrocarbons at different reaction temperatures at $2h^{-1}$ LHSV on Ni@Ce silicate

For comparison, selectivity to C_4 hydrocarbons on the catalyst at various space velocities are plotted in Figs. (**14**, **15**). Fig. (**14**) compares the selectivities at space velocities of $1h^{-1}$ and $2h^{-1}$. Fig. (**14**) shows that the selectivity of C_4 hydrocarbons was higher at lower temperatures (maximum at 250°C), then started decreasing. It is probably due to the formation of highly reactive free radical intermediates at higher temperatures which favors the formation of side products and these are again converted to propylene. The best selectivity results were obtained for these reactions at a space velocity of $5h^{-1}$, as shown in Fig. (**15**). At moderate temperatures, the selectivity of C_4 hydrocarbons was less, and when the temperature was increased the selectivity increased. At lower temperatures and lower residence time the selectivity was low. When the reaction was conducted at a higher temperature with lower residence time, the intermediates are directly contributing to C_4 hydrocarbons. The most useful products obtained in these reactions are n-butanes and iso-butanes which are predominant in the C_4 stream with some butenes as minor products. From the analysis of all the results, the most important observation is the effect of temperature on conversion. In literature most of the reactions are conducted at very high temperatures [16-21, 25-28]. At low temperature, the conversion and selectivity are reported to be too low. But using our nickel catalyst which decreases the activation energy of the reaction, we get >98 % conversions with various product selectivities.

The reaction mechanism behind the ethanol conversion is highly complicated and due to the absence of relevant literature, the explanation is difficult. The plausible reactions on the catalyst surface are shown below. The acidic SiO_2-TaO_2 in the tandem catalyst would act as ethanol dehydration site [34, 35] to produce ethene *in situ*.

$CH_3CH_2OH \longrightarrow CH_4 + H_2 + CO$ [Ni Sites]

$CH_3CH_2OH \longrightarrow CH_2{=}CH_2 + H_2O$ [acidic TaO-SiO_2 sites]

$H_2O + CO \longrightarrow CO_2 + H_2$ [Ni sites]

$CH_2{=}CH_2 + CH_4 \longrightarrow CH_2{=}CH\text{-}CH_3 + H_2$ [Ni-NiO/TaO_2 sites]

$2CH_2{=}CH_2 + H_2 \longrightarrow CH_3CH_2CH_2CH_3 + H_2$ [Ni-NiO/TaO_2 sites]

$CH_3CH_2CH_2CH_3 + CH_4 \longrightarrow CH_3CH_2CH_2CH_2CH_3 + H_2$ [Ni-NiO/TaO_2 sites]

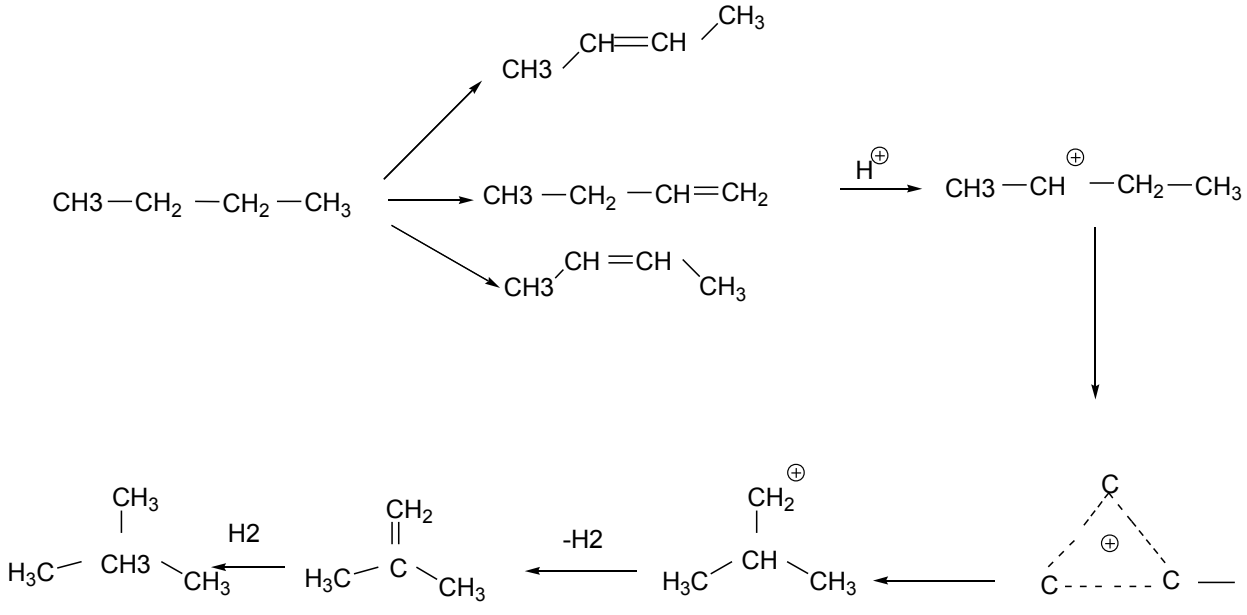

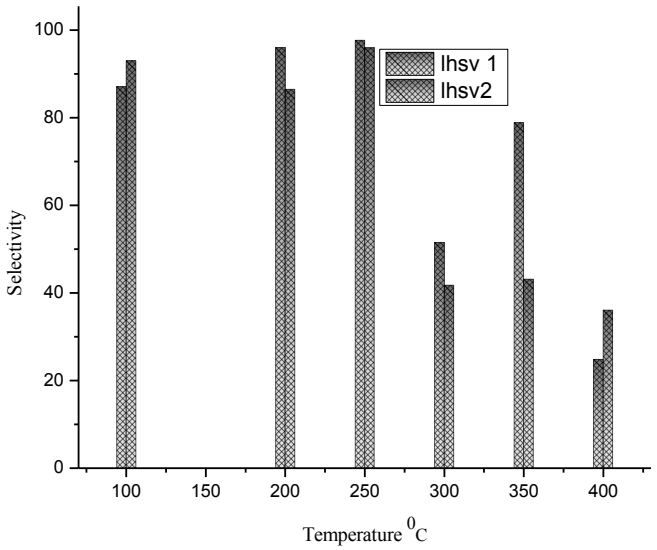

Fig. (14). Selectivity of C_4 hydrocarbons at various reaction temperatures.

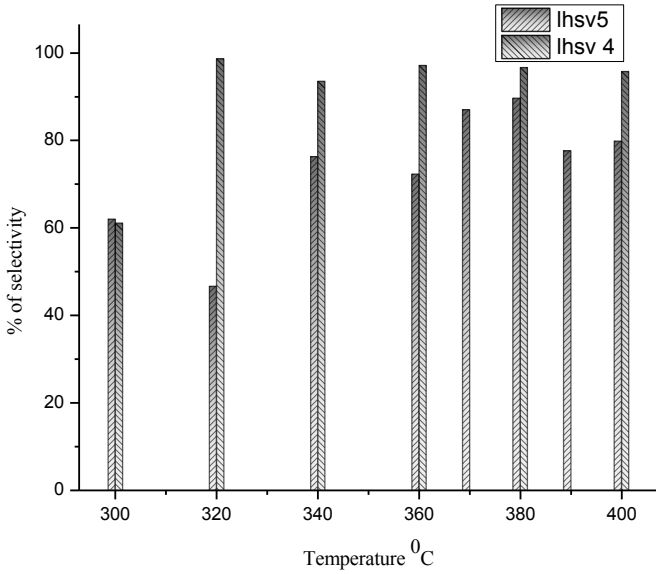

Fig. (15). Selectivity of C_4 hydrocarbons at various temperatures (LHSV 4 & $5h^{-1}$).

Literature reports that these reactions are directed either through carbocation formation or by free radicals. At higher temperatures without the catalyst the dimers, trimers and clusters of carbon are reported *via* the free radical formation from methane. Here, we are also assuming that in the presence of the catalyst these free radicals are formed. This may be the reason for rapid change in the product composition with change in temperature. The isomerized products were obtained on the acid sites of the catalyst through carbocation formation. Dehydration and hydrogenation of the intermediates take place to produce various cis-trans isomers, which is confirmed from the product distribution.

CONCLUSION

Selective synthesis of C_4 hydrocarbons has been achieved on novel mildly acidic core-shell typed Ni@ tantalum silicate catalyst. The extra-large pore system with a multidimensional pore architecture improves the diffusion of straight and branched intermediates and products. Incorporation of nano nickel and tantalum improves the transfer hydrogenation and acidity, respectively. From the detailed study of activity at various temperatures and space velocities, we concluded that temperature plays a crucial role in the production of the intermediates, and the space velocity selectively helps in the formation of C_4 hydrocarbons. The presence of nano nickel particles improves the transfer hydrogenation reaction to stabilize and saturate the products. Mild acidity of the catalyst improves the selectivity of the reaction. One of the most important results in this catalyst system is the high conversion and selectivity at low temperatures. The mechanism of the reaction is complicated and still needs to be studied in detail. The life of the catalyst is also very important for the process, so the catalyst was regenerated by the removal of coke by calcination at high temperature in the presence of oxygen. The original activity of the catalyst was regained after regeneration. We are now focused on doing detailed kinetic study to understand the reaction mechanism and find the life of the catalyst.

CONFLICT OF INTEREST

The authors confirm that this article content has no conflict of interest.

ACKNOWLEDGEMENTS

Director, IIP is acknowledged for approving the work. MGS thanks UGC for research fellowship. The authors thank Analytical Science Division of Indian Institute of Petroleum for analytical services. Funding from CSIR under five-year plan project CSC-0125 is acknowledged.

REFERENCES

[1] Fortman, J.L.; Chhabra, S.; Mukhopadhyay, A.; Chou, H.; Lee, T.S.; Steen, E.; Keasling, J.D. Biofuel alternatives to ethanol: pumping the microbial well. *Trends. Biotechnol.*, **2008**, *26*(7):, 375-381.

[2] Lynd, L.R.; Van Zyl, W.H.; McBride, J.E.; Laser. Consolidated bioprocessing of cellulosic biomass: an update. *Curr. Opin. Biotechnol*., **2005**, *16*, 577-583.

[3] Steen, E.J.; Kang, Y.; Bokinsky, G.; Hu, Z.; Schirmer, A.; McClure, A.; Del Cardayre, S.B.; Keasling, J.D. Microbial production of fatty-acid-derived fuels and chemicals from plant biomass. *Nature*, **2010**, *463*(7280), 559-563.

[4] Kohse-Hoinghaus, K.; Oβwald, P.; Cool, T.A.; Kasper, T.; Hansen, N.; Qi, F.; Westbrook, C.K.; Westmoreland, P.R. Biofuel combustion chemistry: from ethanol to biodiesel. *Angew. Chem. Int. Ed.*, **2010**, *49*, 3572-3597.

[5] Hamelinck, C.K.; Van Hooildonk, G.; Faaij, A.P.C. Ethanol from lignocellulosic biomass: Techno-economic performance in short-, middle- and long-term. *Biomass Bioenerg.*, **2005**, *28*, 384-410.

[6] Sun, Y.; Cheng, J. Hydrolysis of lignocellulosic materials for ethanol production: a review. *Biores. Technol.*, **2001**, *83*, 1-11.

[7] Larsson, S.; Quintana, A.; Sainz, A.; Reimann, N.O.; Jonsson, I.J. Influence of lignocellulose-derived aromatic compounds on oxygen-limited growth and ethanolic fermentation by Saccharomyces cerevisiae. *Appl. Biochem. Biotechnol.*, **2000**, *84/86*, 617-632.

[8] Yu, Z.; Zhang, H. Pretreatments of cellulose pyrolysate for ethanol production by Saccharomyces cerevisiae, Pichia sp. YZ-1 and Zymomonas mobilis. *Biomass Bioenerg.*, **2003**, *24*, 257-262.

[9] Zaldivar, J.; Nielsen, J.; Olsson, L. Fuel ethanol production from lignocellulose: a challenge for metabolic engineering and process integration. *Appl. Microbiol. Biotechnol.*, **2001**, *56*, 17-34.

[10] Xu, J.; Jiang, J.; Hse, C.; Shupe, T.F. Renewable chemical feedstocks from integrated liquefaction processing of lignocellulosic materials using microwave energy. *Green. Chem.*, **2012**, *14*, 2821-2820.

[11] Lu, J.; Sheahanb, C.; Fu, P. Metabolic engineering of algae for fourth generation biofuels production. *Energy Environ*., **2011**, *4*, 2451-2466.

[12] Piccolo, C.; Bezzo, F. 17th European symposium on computer aided process energy. ESCAPE 17, Edited by V. Plesu and P. S. Agachi, Elsevier, **2007**.

[13] Global biofuel out look to 2025, Hart Energy, Texas, USA.

[14] Pamela, P.; Peralta-Yahyu, Zhang, F.; Dei Cardayre, S.B.; Keasling, J.D. Microbial engineering for the production of advanced biofuels. *Nature*, **2012**, *488*, 320-328.

[15] Chu, S.; Majundar, A. Opportunities and challenges for a sustainable energy future. *Nature*, **2012**, *488*, 294-303.

[16] Makshina, E.V.; Janssens, W.; Sels, B.F.; Jacobs, P.A. Catalytic study of the conversion of ethanol into 1,3-butadiene. *Catal. Today*, **2012**, *198*, 338-344.

[17] Jones, M.D.; Keir, C.G.; Lulio, C.D.; Robertson, R.A.M.; Williams, C.V.; Apperley, D.C. Investigations into the conversion of ethanol in to 1,3-butadiene. *Catal. Sci. Technol.*, **2011**, *1*, 267-272.

[18] Bhattaryya, S.K.; Avasthi, B.N. Transformation of ethanol into 1,3-butadiene. *J. Appl. Chem*., **1996**, *16*, 239-244.

[19] Takei, T.; Iguchi, N.; Haruta, M. Synthesis of acetoaldehyde, acetic acid, and others by the dehydrogenation and oxidation of ethanol. *Catal. Surv. Asia*, **2011**, *15*, 80-88.

[20] Abu-Zied, B. M. Structural and catalytic activity studies of silver/chromia catalysts. *Appl. Catal. A. Chem*., *198*, 139-153.

[21] Gazski, A.; Koos, A.; Bansagi, T.; Solymosi, F. Adsorption and decomposition of ethanol on supported Au catalysts. *Catal. Today*, **2011**, *160*, 70-78.

[22] Matsumura, Y.; Hashimoto, K.; Yoshida, S. Selective dehydrogenation of ethanol over highly dehydrated silica. *J. Catal*., **1989**, *117*, 135-143.

[23] Weng, W.; Davies, M.; Whiting, G.; Solsona, B.; Kiely, C. J.; Carley, A. F.; Taylor, S. H. Niobium phosphates as new highly selective catalysts for the oxidative dehydrogenation of ethane. *Phys. Chem. Chem. Phys*., **2011**, *13*(380), 17395-17404.

[24] Lippitis, M.J.; Nieuwenluys, B.E.; Direct conversion of ethanol into ethylene oxide on gold-based catalysts: Effect of CeO_x and LiO_2 addition on the selectivity. *J. Catal*., **2010**, *274*, 142-149.

[25] Goto, D.; Harada, Y.; Furumoto, Y.; Takahashi, A.; Fujitani, T.; Oumi, Y.; Sadakane, M.; Sumo, T. Conversion of ethanol to propylene over HZSM-5 type zeolites containing alkaline earth metals. *Appl. Catal. A. Gen*., **2010**, *383*, 89-95.

[26] Maderia, F.F.; Tayeb, K.B.; Pinard, L.; Vezin, H.; Maury, S.; Cardan, N. Ethanol transformation into hydrocarbons on ZSM-5 zeolites: Influence of Si/Al ratio on catalytic performances and deactivation rate. Study of the radical species role. *Appl. Catal. A. Gen*., **2012**, *443-444*, 171-180.

[27] Tsuchida, T.; Kubo, J.; Yoshioka, T.; Sukuma, S.; Ueada, W. Reaction of ethanol over hydroxyapatite affected byCa/P ratio of catalyst. *J. Catal*., **2008**, *259*, 183-189.

[28] Sen, S.M.; Gurbuz, E. I.; Wettstein, S.G.; Dumesic, D.M.; Maravelias, C.T. Production of butene oligomers as transportation fuels using butene for esterification of levulinic acid from lignocellulosic biomass: process synthesis and technoeconomic evaluation. *Green. Chem*., **2012**, *14*, 3289-3294.

[29] Zhang, H.; Jin, M.; Xia, Y. Noble-metal nanocrystals with concave surfaces: Synthesis and applications. *Angew. Chem. Int. Ed.*, **2012**, 51, 7656-7673.

[30] Deng, Y.; Cai, Y.; San, Z.; Liu, J.; Liu, C.; Wei, J.; Li, W.; Liu, C.; Way, Y.; Zhao, D. Multifunctional mesoporous composite microspheres with well-designed nanostructure: a highly integrated catalyst system. *J. Am. Chem. Soc*., **2010**, *132*, 8466-8473.

[31] http:/www.erm-crm.org. European Reference Materials, Berlin, Germany.

[32] Xingghua, L.; Chun, C.M.; Aksay, I.A.; Shih, W. Synthesis of mesostructured NiO with Silica. *Ind. Eng. Chem. Res*., **2000**, *39*, 684-692.

[33] Bal, R.; Tope, B.B.; Das, T.K.; Hegde, S.G.; Sivasankar, S. Alkali-Loaded Silica, a Solid Base: Investigation by FTIR Spectroscopy of Adsorbed CO2 and Its Catalytic Activity. *J. Catal*., **2001**, *204*, 358-363.

[34] Ushikubo T.; Wada, K. Vapor-phase beckmann rearrangement over silica-supported tantalum oxide catalysts, *J. Catal*. **1994**,*148*, 138-148.

[35] Tanaka, T.; Takenaka, S.; Funabiki, T.; Yoshida, S. Photocatalytic oxidation of ethanol over tantalum oxide supported on silica, studies in surface. *Sci. Catal.*, **1994**, *90*, 485-490.

Received: April 14, 2014 Revised: June 27, 2014 Accepted: August 4, 2014